NUMERICAL SIMULATION OF THE LAGRANGIAN BEHAVIOR OF SOLID PARTICLES IN IMPINGING LIQUID JETS

Edgar A. Matida
Department of Mechanical Engineering & Materials Science
Yokohama National University
79-5 Tokiwadai, Hodogaya-ku, Yokohama-shi 240-8501, Japan

Koichi Nishino
Division of Artificial Environment and Systems
Yokohama National University

Kahoru Torii
Department of Mechanical Engineering & Materials Science
Yokohama National University

ABSTRACT

Lagrangian behaviors of solid particles released in an axisymmetric submerged water jet impinging onto a horizontal plane surface have been studied numerically. The impinging jet flow (Re=13,000) is represented using a modified k-ε turbulence model proposed by Kato and Launder (1993). Trajectories and velocities of the particles are calculated using a one-way coupling Lagrangian eddy-particle interaction model based on Schuen et al. (1983). The assumption of isotropy of local fluid velocity derivatives is made to model the added mass term and the pressure gradient term in the particle equation of motion. Thousands of glass particles (particle to fluid density ratio, ρ_p/ρ_f=2.6) of 1.05 mm diameter are released at the exit of the jet. The mean and root mean square (RMS) velocities of particles simulated are in good agreement with experimental data obtained with a stereoscopic particle tracking technique.

INTRODUCTION

An axisymmetric turbulent jet impinging vertically onto a surface produces high levels of heat and mass transfer in the stagnation region, having many industrial applications, for example, internal cooling of gas turbine blades, cooling of electronic devices and drying of paper and textile products. In some applications, introducing small solid or liquid particles into the flow pursues further augmentation of heat and mass transfer. The impinging jet flow produces highly complex turbulence, exhibiting non-isotropic nature of turbulent fluctuations, strong deceleration of the jet toward the impingement wall, radial acceleration of the wall jet after impingement, steep streamline curvature in the stagnation region and considerable variation of the static pressure in that region. Therefore, impinging jet flows offer a challenging test case for examining overall prediction capability of Lagrangian eddy-particle interaction models to simulate behaviors of particles in turbulent flows.

Before performing simulations of the motion of particles, the turbulent flow itself (primary flow) must be well represented. For its representation, the turbulence models based on the Reynolds averaged Navier-Stokes (RANS) equations have relatively low cost of computation and can be applied to a wide range of geometries and higher Reynolds numbers in comparison with Direct Numerical Simulation (DNS) or Large Eddy Simulation (LES). It is, however, known that the standard k-ε turbulence model produces excessive turbulence energy generation in the stagnation point, leading to high values of turbulence kinetic energy in this region. Kato and Launder (1993) proposed a modified k-ε turbulence model by replacing the generation of turbulence energy by a modified equation, which is shown to lead to more satisfactory predictions in the stagnation region of impinging jets. This model is adopted in the calculation of the primary flow in the present simulation. More advanced and complex models are available in the literature, for example Launder (1996), but they were out of the scope of the present simulation.

Eddy-particle interaction model is a Lagrangian approach used to track particles in the simulation of flows laden with particles. See Grahan and James (1996) for more details. Given initial conditions of velocity and position, the motion of a single particle is calculated by allowing this particle to interact successively with discrete eddies, each eddy having a characteristic size, lifetime and RMS velocity. In order to have velocity statistics, thousands of particles must be released individually in the flow. Their trajectories are calculated by solving the particle equation of motion. When particle concentration is low, the primary flow is not affected by the presence of the particles. This approach is referred to as the one-way coupling. The two-way coupling deals with the mutual interaction between the primary flow and the particles, approach used when concentration of particles is high. The present simulation considers low particle concentration conditions, and hence the one-way coupling

approach is adopted.

Avila and Cervantes (1995) studied numerically the heat transfer augmentation in a turbulent particulate flow. The pipe flow was calculated by using a standard k-ε turbulence model, and the particulate phase was calculated using a Lagrangian eddy-particle interaction model. Shuen et al. (1983) simulated the primary flow, using a k-ε turbulence model and studied the particle dispersion in a turbulent round jet. Most of the previous studies considered only the drag force and the gravity in the particle equation of motion. This approach is valid only when the density ratio between fluid and particles is high (ρ_p/ρ_f>>1).

The present study aims at verifying the applicability of the one-way coupling Lagrangian eddy-particle interaction model to the prediction of behaviors of glass particles released in a submerged water jet impinging onto a horizontal plane surface. The measurement for comparison was done with a stereoscopic particle tracking technique so as to capture highly three-dimensional motions of the particles near the impingement wall. The present paper reports the details of the numerical work, in which the effect of the added mass term and the pressure gradient term in the particle equation of motion is taken into account. These terms, which does not play an important role for the high-density ratio case (ρ_p/ρ_f>>1), were not explicitly examined in most previous predictions. Proper implementation of those terms into the Lagrangian eddy-particle interaction model is proposed, and calculated trajectories and velocities of particles are shown to be in reasonable agreement with the measured results.

IMPINGING WATER JET (PRIMARY FLOW)

The mean velocities, the turbulence kinetic energy and the rate of turbulence dissipation of an impinging water jet flow were calculated using a modified k-ε turbulence model proposed by Kato and Launder (1993).

The production of turbulence kinetic energy, k, is given by

$$P_k = -\overline{u_i u_j} S_{ij}, \tag{1}$$

where the mean strain tensor is defined as

$$S_{ij} = (\partial U_i/\partial x_j + \partial U_j/\partial x_i)/2. \tag{2}$$

On the axis of the impinging jet flow, the symmetry conditions lead to

$$P_k = -2\left(\overline{w'^2} - \overline{u'^2}\right)(\partial U/\partial r), \tag{3}$$

where u and w denote radial and axial (=wall-normal) velocity components, respectively (refer to Fig. 1). Nishino et al. (1996) reported that negative production could occur near the impingement wall where $\overline{u'^2} > \overline{w'^2}$ due to strong inhomogeneity of turbulence. However, the eddy viscosity hypothesis expressed by

$$-\overline{u'_i u'_j} = 2\nu_t S_{ij} - 2k\delta_{ij}/3 \tag{4}$$

results in the following relation:

$$P_k = 2\nu_t S_{ij}^{\ 2}, \tag{5}$$

which is always positive and leads to an excessive production of k near the impingement wall.

In order to circumvent this problem, Kato and Launder (1993) intuitively proposed the use of the following expression for the production of k:

$$P_k = 2\nu_t S\Omega, \tag{6}$$

where $S=(S_{ij}^2)^{1/2}$, $\Omega=(\Omega_{ij}^2)^{1/2}$ and the mean vorticity tensor is defined as

$$\Omega_{ij} = (\partial U_i/\partial x_j - \partial U_j/\partial x_i)/2. \tag{7}$$

As the flow in the stagnation region is basically irrotational, Ω is expected to become small enough to suppress the excessive production of k, while there is little influence on simple shear flows. Fundamental equations for the k-ε model can be expressed by the following equation:

$$\begin{aligned}&\partial(r\phi)/\partial t + \partial(rW\phi)/\partial z + \partial(rU\phi)/\partial r = \\ &\quad \partial\left(r\Gamma\partial\phi/\partial z\right)/\partial z + \partial\left(r\Gamma\partial\phi/\partial r\right)/\partial r + \Sigma.\end{aligned} \tag{8}$$

where ϕ, Γ and Σ are summarized in the Table 1.

Table 1. k-ε model fundamental equations.

Equation (ϕ, Γ, Σ)
Continuity equation (1,0,0)
Component W equation (W, $1/\mathrm{Re}+\nu_t$, $-r\frac{\partial \pi}{\partial z} + \frac{\partial}{\partial z}\left(r\Gamma\frac{\partial W}{\partial z}\right) + \frac{\partial}{\partial r}\left(r\Gamma\frac{\partial U}{\partial z}\right)$)
Component U equation (U, $1/\mathrm{Re}+\nu_t$, $-r\frac{\partial \pi}{\partial r} + \frac{\partial}{\partial z}\left(r\Gamma\frac{\partial W}{\partial r}\right) + \frac{\partial}{\partial r}\left(r\Gamma\frac{\partial U}{\partial r}\right) - 2\Gamma\frac{U}{r}$)
k equation (k, $1/\mathrm{Re}+\nu_t/\sigma_\kappa$, $rP_k - r\varepsilon$)
ε equation (ε, $\nu_t/(\mathrm{Re}\,\sigma_\varepsilon)$, $rC_1P_k\varepsilon/k - rC_2\varepsilon^2/k$)

where $\pi = \overline{p} + 2k/3$, $\nu_t = C_\mu k^2/\varepsilon$, $C_\mu = 0.09$, $C_1 = 1.44$, $C_2 = 1.92$, $\sigma_k = 1.0$ and $\sigma_\varepsilon = 1.3$.

Equations are solved using structured grid (89x129 grid points), staggered mesh and SIMPLE method. Equations were discretized by using finite volumetric method, in the convection terms QUICK scheme are used. Calculations were performed for a submerged water jet with a Reynolds number of approximately 13,000 based on nozzle diameter (D=40.0 mm) and nozzle exit velocity (W_0*=0.3 m/s). The distance of the nozzle and the impingement wall was 234.0 mm. The nozzle plate has a radius of 400.0 mm and sidewall is placed at a radius of 475.0 mm from the jet axis. These conditions were the same as the flow turbulence statistics measurements made by Nishino et al. (1996). See Fig. 1 for the schematic view of the experimental apparatus. For the inlet boundary conditions, a top-hat mean velocity profile is adopted (W/W_0*=1, U/W_0*=0), while k/W_0*^{2}=0.008 and the

$\varepsilon D/W_0^{*3}$=0.00015 are used. For the outlet boundary conditions, $\partial\phi/\partial z$=0 (ϕ=W, U, k and ε) is assumed. The simulations are done on the half flow domain with symmetry boundary conditions on the axis of the jet. The wall-function relation is imposed on the solid wall.

Figure 2 shows the axial distribution of the calculated and the measured axial and radial mean velocities of the fluid flow at four radial locations r/D=0.125, 0.225, 0.625 and 0.875. The turbulence kinetic energy is also plotted here. The calculated fluid velocities W_f/W_0^* and U_f/W_0^* are in good agreement with those measured at these particular r/D. Although not shown here, there is also good agreement for the entire impinging jet flow region, except for the region very near to the impingement wall.

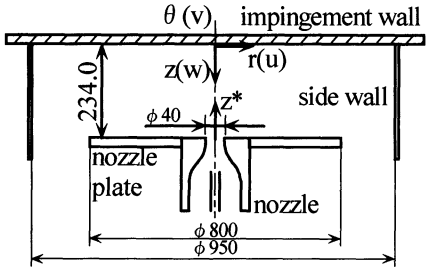

Figure 1. Details of impinging jet flow geometry.

PARTICLE EQUATION OF MOTION

Tchen extended the work of Basset, Boussinesq and Ossen and proposed an equation for the motion of a rigid sphere in a nonuniform flow (see Hinze, 1975). After rigorous analysis, Maxey and Riley (1983) proposed an equation of motion of a small sphere with relative motion of low Reynolds number. Recently, Kim et al. (1998) proposed new equations for the particle motion superior to the previous equations and valid for Re_p=2∼150 and ρ_p/ρ_f=2∼200. Neglecting some terms and considering the drag force, the added mass, the pressure terms and the gravity, the Lagrangian equations that describe the movement of particles in the cylindrical coordinate system are

$$\frac{du_p}{dt}=\frac{(u_f-u_p)}{\tau_p}+\frac{\rho_f}{2\rho_p}\left(\frac{Du_f}{Dt}-\frac{v_f^2}{r_p}-\frac{du_p}{dt}\right)+\frac{\rho_f}{\rho_p}\left(\frac{Du_f}{Dt}-\frac{v_f^2}{r_p}\right)+\frac{v_p^2}{r_p} \tag{9}$$

$$\frac{dv_p}{dt}=\frac{(v_f-v_p)}{\tau_p}+\frac{\rho_f}{2\rho_p}\left(\frac{Dv_f}{Dt}+\frac{u_fv_f}{r_p}-\frac{dv_p}{dt}\right)+\frac{\rho_f}{\rho_p}\left(\frac{Dv_f}{Dt}+\frac{u_fv_f}{r_p}\right)-\frac{u_pv_p}{r_p} \tag{10}$$

$$\frac{dw_p}{dt}=\frac{(w_f-w_p)}{\tau_p}+\frac{\rho_f}{2\rho_p}\left(\frac{Dw_f}{Dt}-\frac{dw_p}{dt}\right)+\frac{\rho_f}{\rho_p}\frac{Dw_f}{Dt}+g\left(1-\frac{\rho_f}{\rho_p}\right) \tag{11}$$

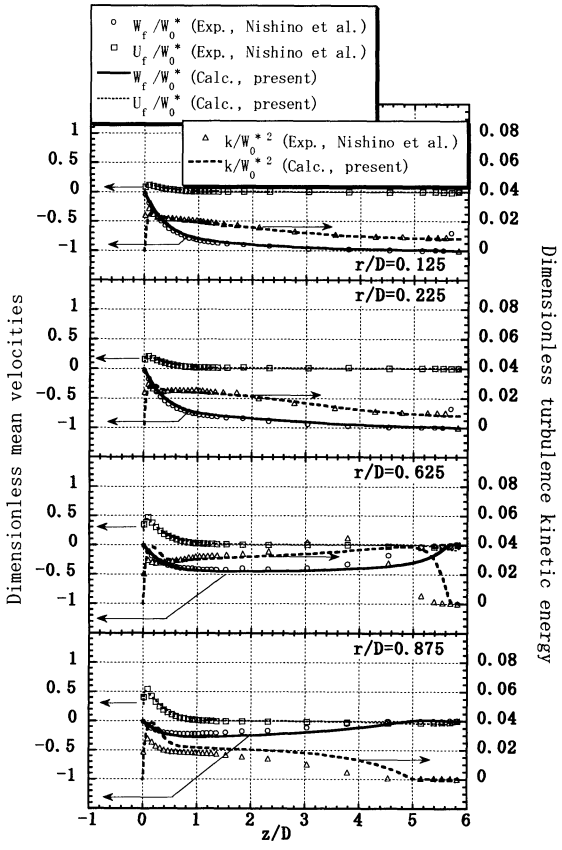

Figure 2. Axial distributions of calculated and measured axial mean velocity, radial mean velocity and turbulence kinetic energy of the fluid flow.

where, $\tau_p=\dfrac{d_p^2\rho_f}{18fv_f\rho_p}$, $f=1+0.15\mathrm{Re}_p^{0.687}$, $\mathrm{Re}_p=\dfrac{d_pu_r}{v_f}$,

and $u_r=((u_f-u_p)^2+(v_f-v_p)^2+(w_f-w_p)^2)^{1/2}$.

Here, subscript p and f denote particle and fluid, respectively. The terms representing centrifugal forces v_p^2/r_p and the conservation of angular momentum $-u_pv_p/r_p$ appear in the equations for u_p and v_p, respectively. Although the time derivative (for example, in the axial direction) should be represented by

$$\frac{Dw_f}{Dt}\equiv\frac{\partial w_f}{\partial t}+u_f\frac{\partial w_f}{\partial r}+\frac{v_f}{r}\frac{\partial w_f}{\partial\theta}+w_f\frac{\partial w_f}{\partial z}, \tag{12}$$

the use of

$$\frac{dw_f}{dt}\equiv\frac{\partial w_f}{\partial t}+u_p\frac{\partial w_f}{\partial r}+\frac{v_p}{r}\frac{\partial w_f}{\partial\theta}+w_p\frac{\partial w_f}{\partial z}, \tag{13}$$

as proposed by Buevich (1966) is found to lead to more satisfactory results of RMS velocities of particles. In consequence, the following substitution is made on Eqs.(9)-(11):

$$\frac{Du_f}{Dt} \to \frac{du_f}{dt}, \quad \frac{Dv_f}{Dt} \to \frac{dv_f}{dt} \quad \text{and} \quad \frac{Dw_f}{Dt} \to \frac{dw_f}{dt}. \quad (14)$$

The local gradient of the mean fluid velocities is determined from linear interpolation of the mean fluid velocities obtained at neighboring grid points in the k-ε turbulence model calculation. Assuming isotropic conditions, the fluctuating values of the time derivative and the local velocity gradients are calculated from a Gaussian probabilistic distribution with the following standard deviations:

$$(\partial w'_f/\partial t)_{rms} = (\varepsilon W_f^2/15\nu)^{1/2}, \quad (15)$$

$$(\partial w'/\partial z)_{rms} = (\varepsilon/15\nu)^{1/2} \text{ and} \quad (16)$$

$$(\partial w'/\partial r)_{rms} = (r^{-1}\partial w'/\partial\theta)_{rms} = (2\varepsilon/15\nu)^{1/2}. \quad (17)$$

The corresponding quantities in the radial and azimuthal directions can be represented in the same way. The local velocity gradients are first calculated in the Cartesian coordinates and then transformed to the cylindrical coordinates.

LAGRANGIAN EDDY-PARTICLE INTERACTION MODEL

Given initial conditions of velocity and position, the motion of a single particle is calculated by allowing this particle to interact successively with discrete eddies, each eddy having a characteristic size, lifetime and RMS velocity. At the start of a certain eddy-particle interaction, the particle with initial velocity, u_{p0}, is located at the center of an eddy with a characteristic velocity, u_e. The eddy translates with the instantaneous local fluid velocity, but the particle, according to its equation of motion, will have another trajectory, which is not coincident with the center of the eddy. A new interaction starts when the eddy lifetime is over or the particle crosses the eddy.

Based on Schuen et al. (1983), the following characteristic scales were adopted:

$$\tau_e = 0.2k/\varepsilon, \; L_e = 0.164k^{1.5}/\varepsilon \text{ and } u_e = \sqrt{2k/3}. \quad (18)$$

Fluid velocity fluctuations are generated by

$$(u'_f, v'_f, w'_f) = (u_e N_u, u_e N_v, u_e N_w), \quad (19)$$

where N_u, N_v and N_w are random numbers generated from a Gaussian probability density distribution with zero mean and unity standard deviation. The generated fluctuations remain constant during the particle-eddy interaction considered.

The time of interaction between particle and eddy is given by

$$\tau_i = \min(\tau_e, \tau_c), \quad (20)$$

where the crossing time is estimated from

$$\tau_c = L_e/u_r. \quad (21)$$

Here, u_r is evaluated at the start of interaction.

EXPERIMENT

Motions of spherical glass particles (ρ_p/ρ_f=2.6) 1.05±0.15 mm in diameter released in a submerged impinging water jet (Re=13,000) were measured to provide experimental data comparable with the present simulation results. The details of the experimental facility are found in the report by Nishino et al. (1996) (see again Fig. 1). Particles mixed with water in an auxiliary tank were introduced inside the nozzle via a fine tube located at 55 mm upstream of the nozzle mouth. The volumetric particle concentration in the auxiliary tank was about 0.1 %. The particles suspended in the water jet were issued vertically upward from the nozzle.

A pulsed light with HMFW duration of 18～25 μs generated by a stroboscope was used to illuminate a 3-D flow domain between the nozzle exit and the impingement wall. Stereoscopic observation was made of the motions of the particles by using two CCD cameras simultaneously. The viewing angle between the cameras was 60 degrees. A frame grabber which is PCI-interfaced with a host PC captured analog TV frames in real time. Consecutive 120 frames digitized at 60 fps were stored in a hard disk drive.

After experiment, digital image processing was applied to determine the centroidal position of each particle image recognized in digitized frames. The displacement of the centroidal position was tracked to establish its 2-D trajectory. Stereo-pair matching was finally done to reconstruct 3-D trajectory. These procedures were basically the same as those of Kato et al. (1995) except that only those trajectories that were tracked successfully for more than 30 frames were retained as data. More details of the experiment will be reported elsewhere.

CALCULATION RESULTS

Figure 3(a) shows three-dimensional trajectories of 1.05 mm particles obtained experimentally. Note that the impingement wall is placed at z/D=0 and the center of the nozzle exit at z/D=5.85. Calculated trajectories for 15 particles released at z/D=5.0 and random radial locations (r/D<5) are shown in Fig. 3(b). Particles travel upward in relatively smooth lines until the region near the impingement wall, follow the streamline curvature of the water flow and then fall due to the effect of gravity. Trajectories in the top-view plot show random zigzag movement in the radial direction near the stagnation point. There is a qualitative agreement between the calculation and the experiment. Some particles in the experiment and also in the calculation have arrived at and impinged onto the wall.

Figure 4 shows the axial distributions of the dimensionless axial (a) and radial (b) mean velocities at r/D=0.125, 0.225, 0.625 and 0.875. Here, comparison between the calculation and the experiment is made for the particle velocities (W_p/W_0* and U_p/W_0*). For reference, the calculated fluid velocities (W_f/W_0* and U_f/W_0*) are shown in dotted lines. The calculation for the axial mean velocities of particles (see "W_p/W_0* (Calc., all terms)" in the figure) is in relatively good agreement with those measured. Particles are going upward with an axial mean velocity lower than the

fluid mean velocity because of the gravity effect. Also shown in the figure as "W_p/W_0* (Calc., drag)" is the result neglecting both the added mass term and the pressure term in the particle equation of motion. This simplification appears to have little influence on the prediction of the axial mean velocities of particles. Note that similarly good agreement between the calculation and the experiment is shown in the radial mean velocity.

Figure 5 presents the axial distributions of the dimensionless axial (a) and radial (b) RMS velocities at various *r/D*. The inclusion of the added mass term and the pressure term in the particle equation of motion is crucial to predict well the axial RMS velocities of particles, as evident from the comparison between the prediction neglecting those terms and the experiment.. Fig.5 (b) shows that the RMS values of radial particle velocity fluctuations are also predicted reasonably in the present calculation.

The dimensionless mean product of the axial and radial velocity fluctuations of particles is plotted in Fig.6. An interesting feature recognized here is the lack of correlation in the particle velocities (u'_p and w'_p) even though there is strong correlation in the fluid velocities (u'_f and w'_f). The lack of correlation seems to support the random-interaction treatment made in the Lagrangian eddy-particle interaction model. Present calculation is in good agreement with the

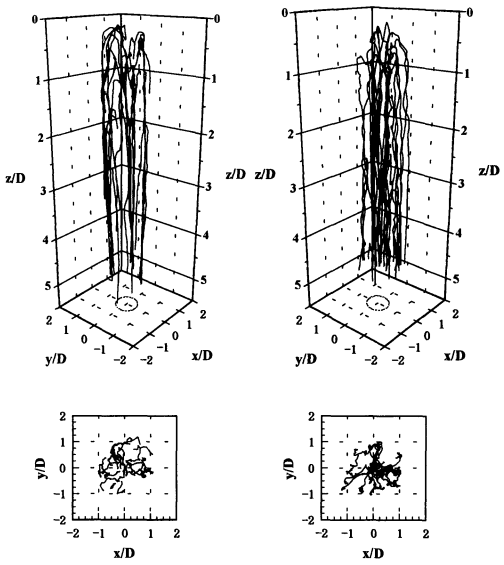

Figure 3. Measured (a) and calculated (b) trajectories of 1.05 mm glass particles in impinging water jets (Re=13,000); bird's-eye plot and top-view plot.

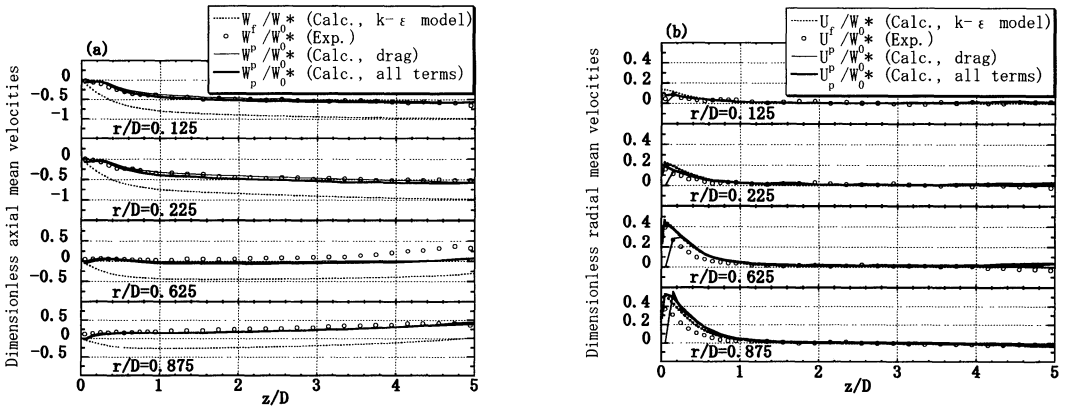

Figure 4. Experimental and calculated axial distributions of axial (a) and radial (b) mean velocities of particles and fluid.

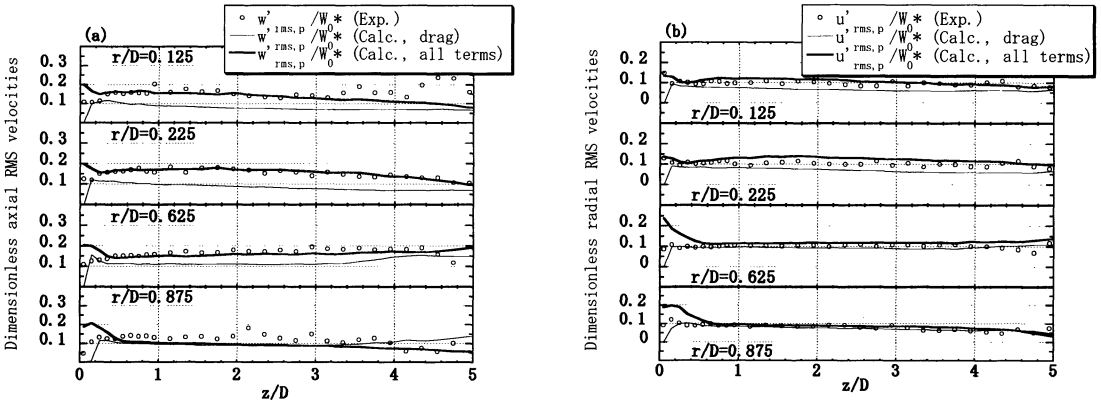

Figure 5. Experimental and calculated axial distributions of axial (a) and radial (b) RMS velocities of particles and fluid.

experiment, except for the region very close to the impingement wall, where the prediction of turbulence of the primary flow by the k-ε model decreases its accuracy.

Figure 7 gives the radial dispersion of particles relative to their mean trajectory. The radial dispersion is defined as the mean-square of the radial distance between individual particle location and ensemble-averaged particle location at a certain time lag after particles have passed through a fixed starting region in the flow field. Two starting regions, (z/D,r/D)=(2.45～2.5,0.1～0.15) and (2.45～2.5,0.2～0.25) are chosen here. It is shown that for a time lag less than 0.7 s, the calculation is in good agreement with the measurement, but in the long term, calculated dispersion starts to deviate from the experiment. Note that there is a time where dispersion becomes constant, indicating that particles have reach the impingement wall region and have started to fall under gravity effect.

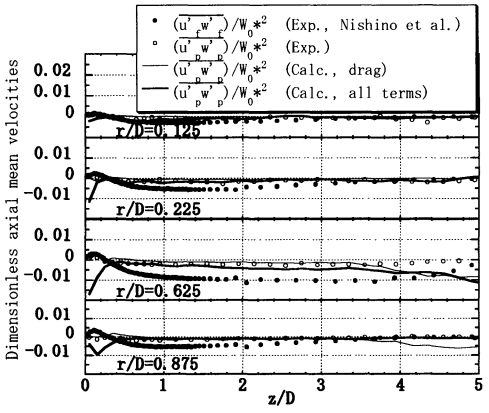

Figure 6. Experimental and calculated axial distributions of mean stresses of particles and fluid.

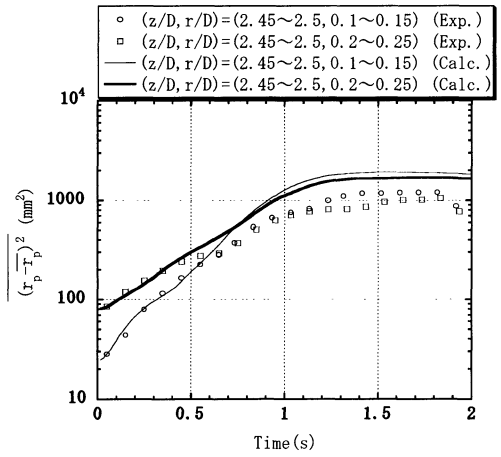

Figure 7. Dispersion of particles relative to their mean trajectories starting from two particular locations.

CONCLUSIONS

The motions of glass particles (d_p=1.05 mm, ρ_p/ρ_f=2.6) in a submerged vertical impinging water jet have been studied numerically using a Lagrangian one-way coupling eddy-particle interaction model. The added mass and pressure gradient terms are considered in the particle equation of motion and modeled into the Lagrangian simulation by assuming the isotropy of the velocity derivatives. The simulated results are compared with the experimental data obtained with a stereoscopic particle tracking technique. It is shown that the particles travel in relatively smooth lines until the region close to the impingement wall where the particles start to behave in highly turbulent manner. Simulated values of axial and radial mean velocities of particles are in good agreement with those of experiment. Also good agreement is obtained for the fluctuating velocities of particles only when the and added mass and pressure gradient terms are considered in the simulation. The lack of correlation between axial and radial velocity fluctuations of particles is experimentally pointed out to support the hypothesis made in the Lagrangian simulation.

ACKNOWLEDGEMENTS

This work was supported by Grant-in-Aid for Scientific Research Project (C) (No. 09650230) of the Ministry of Education, Science, Sports and Culture of Japan.

REFERENCES

Avila, R. and Cervantes, J., 1995, "Analysis of the Heat Transfer Coefficient in a Turbulent Particle Pipe Flow," *Int. Journal of Heat and Mass Transfer*, Vol. 38, No. 11, pp. 1923-1932.

Buevich, Y. A., 1966, "Motion Resistence of a Particle Suspended in a Turbulent Medium", *Fluid Dynamics*, Vol. 1, pp. 119.

Grahan, D. I. and James, P. W., 1996, "Turbulent Dispersion of Particles Using Eddy Interaction Models," *Int. Journal of Multiphase Flow*, Vol. 22, No. 1, pp. 157-175.

Hinze, J. O., 1975, "Turbulence," McGraw-Hill, New York, pp. 460-471.

Kato, M. and Launder, B. E., 1993, "The Modeling of Turbulent Flow Around Stationary and Vibrating Square Cylinders," *9th Symp. Turb. Shear Flows*, pp. (10-4-1)-(10-4-6).

Kato, H., Nishino, K., Shinshi, A. and Torii, K., 1995, "Measurement of Velocity and Size of Particles by Using Stereo-Imaging Technique," ASME FED-Vol.209, Flow Visualization and Image Processing of Multiphase Systems, Yang, W. J. et al. (eds.), Book No.G00959-1995, pp.115-122.

Kim, I., Elgobashi, S. and Sirignano, W. A., 1998, "On the Equation for Spherical-Particle Motion: Effect of Reynolds and Acceleration Numbers," *Journal of Fluid Mechanics*, Vol. 367, pp. 221-253.

Launder, B. E., 1996, "Turbulence and Transition Modeling," M. Hallback et al. (eds.), Kluwer Academic Publishers, Netherlands, Chapter 5, pp. 193-231.

Maxey, M. R. and Riley, J. J., 1983, "Equation of Motion for a Small Rigid Sphere in a Nonuniform Flow". *Physics Fluids*, Vol. 26, pp. 883-889.

Nishino, K., Samada, M., Kasuya, K. and Torii, K., 1996, "Turbulence Statistics in the Stagnation Region of an Axisymmetric Impinging Jet Flow," *Int. Journal of Heat and Fluid Flow*, Vol. 17, pp. 193-201.

Schuen, J. S., Chen, L. D. and Faeth, G. M., 1983, "Evaluation of a Stochastic Model of Particle Dispersion in a Turbulent Round Jet," *AIChE Journal*, Vol. 29, pp. 167-170.